Journal of Solid State Chemistry 184 (2011) 1016–1024

Contents lists available at ScienceDirect

Journal of Solid State Chemistry

journal homepage: www.elsevier.com/locate/jssc

Thermodynamical and structural insights of orange II adsorption by Mg_RAlNO_3 layered double hydroxides

Mohamed Mustapha Bouhent [a,b], Zoubir Derriche [a,*], Renaud Denoyel [c], Vanessa Prevot [b], Claude Forano [b]

[a] Laboratoire de Physico-Chimie des Matériaux, Catalyse et Environnement, UST d'Oran, Bp 1505 Oran El M'naouer, Algérie
[b] Laboratoire des Matériaux Inorganiques, UMR CNRS 6002, Université Blaise Pascal, F-63177 Aubière Cedex, France
[c] MADIREL, Laboratoire Chimie Provence, Université d'Aix-Marseille I, II et III, UMR CNRS 6264, Campus de Saint Jérôme, Avenue Escadrille-Normandie-Niemen, F-13397 Marseille Cedex 20, France

ARTICLE INFO

Article history:
Received 7 December 2010
Received in revised form
2 March 2011
Accepted 6 March 2011
Available online 15 March 2011

Keywords:
Layered double hydroxides
Dye
Intercalation
Adsorption isotherm
Thermodynamic constants

ABSTRACT

$[Mg_{1-x}\ Al_x(OH)_2][(NO_3)_x, nH_2O]$ Layered Double Hydroxide (LDH) sorbents with variable Mg/Al molar ($R=(1-x)/x$) ratios were investigated for adsorption of azo dye, orange II (OII) at various pH and temperature conditions. Mg_2AlNO_3 displays the highest adsorption capacity with 3.611 mmol of OII per gram of Mg_2AlNO_3 at 40 °C. Adsorption isotherms have been fitted using the Langmuir model and free energy of adsorption (ΔG°), enthalpy (ΔH°) and entropy (ΔS°) were calculated. The experimental values for ΔG° in temperature range between 10 and 40 °C were found to be negative indicating that a spontaneous process occurred. Positive calculated enthalpy values, characteristic of an endothermic process were found. Characterization of solids (PXRD, FTIR, UV–vis, TGA/DTA, adsorption isotherm BET analysis, SEM and Zetametry) before and after adsorption showed that adsorption proceeds in two steps. First, adsorption occurs at the LDH surface, followed by intercalation via anion exchange.

© 2011 Elsevier Inc. All rights reserved.

1. Introduction

Discharging large amount of dyes in water resources from various dyestuff manufactures, plastic, and paper making industries, pose some hazards and environmental problems.

Color, which is easily detected, is the first characteristics of such effluent. The presence of dye in water affect its nature, inhibiting sunlight penetration into stream and reducing the photosynthetic reaction [1]. Majority of dyes are composed of aromatic rings in their structure, rendering them mutagenic and carcinogenic [2]. Color removal is a major problem because most dyes are resistant to biological degradation due to their complex structure and xenobiotic properties. Adsorption techniques using various sorbents such as activated carbons [3], fly-ashes [4], woods [5], piths [6], and clays [7–9], provide an attractive alternative in removing colored organic species, in term of initial cost, simplicity of design, ease of operation and insensitivity to toxic substances comparatively to biotechnological processes. Due to their easily preparation and regeneration, clay derivatives are among the most appropriate sorbents [10,11].

Due to their unique anion exchange properties [12,13], Layered Double Hydroxides (LDH) also called anionic clays [14] have received increased interest in the recent decade for the purpose of environmental remediation processes [15], as ionophore-like compounds in potentiometric sensors and biosensors [16,17] and especially for removal of dyes [18–22]. The structure of these materials is based on the stacking of brucite $[Mg(OH)_2]$-like layers, where partial substitution of trivalent for divalent metal ions leads to positive layer charges balanced by interlayer hydrated anions. The general formula of LDH is represented by $[M^{II}_{1-x}\ M^{III}x(OH)_2]^{x+}[X^{q-}_{x/q},\ nH_2O]^{x-}$ [23,24], where M^{II} and M^{III} represent the divalent and trivalent cation, respectively, X is the interlayer anion, and q is the charge of the interlayer anion. The most studied class of LDH is the hydrotalcite-like compounds, MgAlX with M^{II}=Mg, M^{III}=Al and $X^{q-}=CO_3^{2-}$, Cl^-, NO_3^-, and SO_4^{2-}. Compared to divalent anions, monovalent anions are more easily replaced by almost any organic or inorganic anions, by anion exchange [13,25]. For $MgAlNO_3$, nitrates can be exchanged more easily than other simple inorganic anions, such as Cl^-, OH^- and CO_3^{2-} and the materials can be easily prepared using Al and Mg nitrate salts.

Most papers published on the adsorption of organic chemicals (dye molecules, pesticides, and drugs) as inorganic adsorbents deals with clays, metal phosphates, metal oxide and hydroxides. These papers focused on the experimental measurements of

* Corresponding author.
E-mail address: derriche_zoubir@yahoo.com (Z. Derriche).

0022-4596/$ - see front matter © 2011 Elsevier Inc. All rights reserved.
doi:10.1016/j.jssc.2011.03.018

adsorption isotherms for the determination of the adsorption capacities of the solids and comparison of their properties. This approach requires the thermodynamic model to best fit the isotherm plots. Many models, described in the literature, have been used such as the so-called Langmuir, Freundlich, Temkin and Redlich–Peterson models, which are based on different assumptions concerning the adsorbat–adsorbent interactions. The need is then great to determine thermodynamic parameters, such as ΔG^0_{ads}, ΔH^0_{ads}, and ΔS^0_{ads} from these models. Moreover, while such models are devoted to physisorption processes of neutral molecules they are used indiscriminately for cationic or anionic molecules, polymers or even nanometer size biomolecules such as enzymes. Therefore, the objective of the current study was to evaluate the efficiency of Mg_RAlNO_3 for the uptake of OII at different conditions of equilibrium concentrations. Furthermore, the adsorption properties were quantified for different stoichiometries of Mg_RAlNO_3 sorbents (R=Mg/Al=2, 3, 4), and for different parameters such as temperature and pH. Insight in the thermodynamic of the adsorption process was performed through modelization of the adsorption isotherms in order to validate these models for the calculation of adsorption energy. Finally, guest–host interactions are discussed on the basis of XRD, ATR–FTIR and UV–Visible diffuse reflectance spectroscopy.

2. Experiment

2.1. Materials and preparations

Materials: For all preparations, the magnesium and aluminum nitrate salts were of analytical grade (Acros). The acid orange 7 also referred as orange II (OII) of chemical formula $C_{16}H_{12}N_2O_4SNa$ (Fig. SI-1) was supplied by Aldrich Chemical. Deionised water was used for all experiments.

Preparation of Mg_RAlNO_3: The nitrate containing hydrotalcite-like compounds (Mg_RAlNO_3 LDH) were prepared by the coprecipitation method at controlled pH [26,27]. The materials were coprecipitated by the simultaneous dropwise addition of a magnesium and aluminum nitrate mixed aqueous solution (total metal concentration equal to ΣM=1 mol/L) with Mg^{2+}/Al^{3+} molar ratios R=2, 3 and 4 and a NaOH aqueous solution (2 mol/L). The addition rate of the alkaline solution was regulated in order to keep the pH constant at 10.0 ± 0.3. The reactions were carried out at 25 ± 1 °C under N_2 to minimize CO_3^{2-} contamination from atmospheric CO_2. The resulting precipitates were left 12 h for ageing and then separated by three repeated washing/centrifugation cycles. The products were finally dried at room temperature.

2.2. Characterization of solids

Chemical analyses (Mg, Al, C, H, S, and N) were performed at the Vernaison Analysis Center of CNRS. The powder X-ray diffraction (PXRD) patterns of the solid samples were recorded using Siemens D501 diffractometer with Cu $K\alpha$ radiation (λ=0.15415 nm). Patterns were recorded over the 2–70 2θ range in steps of 0.04° with a counting time per step of 8 s. Attenuated Total Reflectance Fourier Transform infrared (ATR–FTIR) spectra were measured in the range 400–4000 cm^{-1} on a FTIR Nicolet 5700 (Thermo Electon Corporation) spectrometer equipped with a Smart Orbit accessory. The UV–vis spectra were recorded with a Nicolet evolution 500 spectrometer in the spectral window from 190 to 900 nm. Differential thermal/thermogravimetric (DTA/TGA) analyses were performed using a Setaram TGA92 thermogravimetric analyzer in the temperature range of 25–1050 °C, with a heating rate of 5 °C/min, under air atmosphere. Scanning electron micrographs were recorded with a LEO Stereoscan microscope at 15 KV at the CASIMIR Laboratory. The nitrogen adsorption/desorption isotherms were recorded on a Fison SP 1920, after outgassing of materials at 80 °C for 12 h. Particle size analysis were performed by dynamic light scattering technique using the Zetasizer nano ZS from Malvern. Zeta potential measurements using laser Doppler electrophoresis (LDE) were realized using the same apparatus. UV–Visible diffuse reflectance spectroscopy analysis was performed using an Evolution 500 UV–Visible spectrophotometer from Nicolet fitted with a RSA-UC-40 diffuse reflectance integrating sphere.

2.3. Sorption experiments

OII sorption experiments were carried out using a batch method at a controlled temperature of 20 °C. The adsorption isotherms were recorded for 50 mL of 1 mg/mL solid suspensions in equilibrium with OII concentrations ranging from 0 to 5.7 mmol/L. The pH was initially fixed at 7.0 ± 0.5 by addition of either HCl or NaOH 0.1 M solution. The suspensions were stirred at a constant speed (500 rpm) for 12 h and centrifuged at 4500 rpm for 30 min. Dye concentration was estimated spectrophotometrically by monitoring the absorbance at λ max=483 nm (Fig. SI-1). The amount of OII adsorbed by the clays, q_e, was determined from the difference between the initial (C_i) and equilibrium (C_e) concentrations of the dye per gram of LDH: $q_e=(C_i-C_e)V/m$. The adsorption isotherms were obtained by plotting q_e versus C_e. Adsorption isotherms were systematically repeated three times.

3. Results and discussion

3.1. Chemical, structural and textural characterization of Mg_RAl LDH sorbents.

In order to better understand the adsorption behaviors of the Mg_RAl LDH phases toward the dye molecule, a fine characterization of their structural and textural properties has been performed.

The chemical compositions and the anion exchange capacities of Mg_RAlNO_3 LDH compounds are presented in Table 1. The experimental Mg^{2+} and Al^{3+} solid contents determinated by ICP, are close to the expected values, thus indicating the usefullness of the constant pH coprecipitation method for the preparation of LDH material in order to obtain the desired composition. We note a slight but often-unavoidable contamination with carbonate anions.

Table 1
Chemical compositions of Mg_RAlNO_3 LDH.

R	Mg^{2+}/Al^{3+}	$\Sigma(NO_3^- + CO_3^{2-})/Al^{3+}$	%H_2O	Chemical formula	A.E.C.[a] m_{eq}/100 g	Abbreviation
2	2.00	1.00	12.08	$Mg_{0.33}Al_{0.66}(OH)_2(NO_3)_{0.29}(CO_3)_{0.02}$ 1.77H_2O	373.7	Mg_2AlNO_3
3	2.92	0.99	12.66	$Mg_{0.73}Al_{0.25}(OH)_{1.96}(NO_3)_{0.21}(CO_3)_{0.02}$ 2.35H_2O	301.8	Mg_3Al NO_3
4	3.88	1.00	14.95	$Mg_{0.77}Al_{0.20}(OH)_{1.95}(NO_3)_{0.18}(CO_3)_{0.01}3.6H_2O$	245.8	Mg_4Al NO_3

[a] Calculated for the hydrated materials.

Chemical formulae for Mg_RAlNO_3 are close to those calculated with a number of water molecules determinated by DTA/TG, just necessary to fill all the available interlayer crystallographic sites [28].

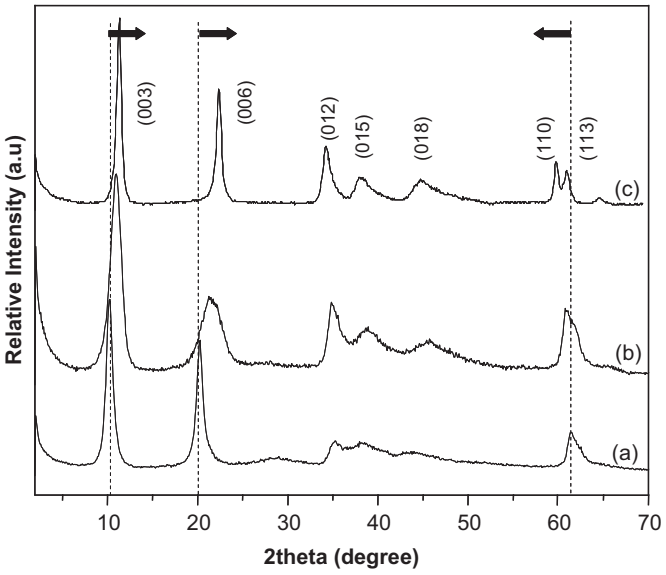

Fig. 1. XRD patterns of (a) Mg_2AlNO_3, (b) Mg_3AlNO_3, and (c) Mg_4AlNO_3 LDH phases.

Table 2
Structural and textural data for Mg_RAlNO_3 LDH phases.

Compounds	a (nm)	c (nm)	d_{bs} (nm)	d_{Gal}[a] (nm)	S_{BET} ($m^2\,g^{-1}$)	Mean particle size (nm)
Mg_2AlNO_3	0.3005(2)	2.7090(5)	0.9030	0.426	26	602
Mg_3AlNO_3	0.3043(3)	2.4360(6)	0.8120	0.335	32	555
Mg_4AlNO_3	0.3060(2)	2.3700(3)	0.7900	0.316	37	472

[a] Calculated from $d_{Gal}=d_{bs}-d_{bs}(\text{brucite})=d_{bs}-0.477$.

XRD patterns of the Mg_RAlNO_3 LDH precursors ($R=2$, 3, 4) display the characteristic X-ray reflections (Fig. 1A) of the hexagonal R-3 m hydrotalcite mineral group [13]. No crystalline $Mg(OH)_2$ or $Al(OH)_3$ phase was detected. The basal spacings were determined to be 0.903, 0.812 and 0.790 nm for Mg_2AlNO_3, Mg_3AlNO_3 and Mg_4AlNO_3, respectively (Table 2).

The progressive decrease of the basal spacings from Mg_2Al to Mg_4Al accounts for the decrease of the anion exchange capacities and the subsequent rearrangement of the nitrate anions. The gallery heights, calculated from the difference between LDH and Brucite (0.477 nm) basal spacings are 0.426, 0.335 and 0.313 nm, respectively, for Mg_2AlNO_3, Mg_3AlNO_3 and Mg_4AlNO_3. This supposes that the nitrate anions (ionic diameter ≈ 0.4 nm) are in a nearly of perpendicular orientation toward the layers for Mg_2AlNO_3 while they may lie flat in the Mg_4AlNO_3 phase [28]. Consequently, a more ordered structure is observed for Mg_4AlNO_3–LDH compared to Mg_3AlNO_3–LDH and Mg_2AlNO_3–LDH leading to an increase of cristallinity as shown by the sharpening of the full width at half maximum of the diffraction lines (Fig. 1).

ATR–FTIR analysis also evidences the structural difference between Mg_4Al compound and both Mg_2Al and Mg_3Al phases (Fig. 2). For the Mg_4Al adsorbent, NO_3^- anions display in the 1300–1500 cm^{-1} region a single band (antisymmetric stretching mode ν_3, 90%), corresponding to nitrate species with a high molecular symmetry (D_{3h}). When it is intercalated in Mg_2Al and Mg_3Al, two bands are clearly observed due to a lowering of the symmetry to C_{2V}. Simultaneously, the rearrangement of intercalated nitrate anions leads to a strong modification of the ν_{OH} stretching band feature between 3000 and 3800 cm^{-1}. The decrease of the relative intensity of the ν_{as}OH and ν_sOH bands of H_2O compared to the intensity of the νMO–H band (doublet) clearly indicates that the amount of intercalated water molecules has been reduced due to the rearrangement of the anions and the interlayer contraction. A new νOH band characteristic of free MO–H group appears at higher energy (3681 cm^{-1}).

Bands at around 700–400 cm^{-1} can be attributed to the Al–OH and Mg–Al–OH bending vibrations of the LDH lattice. Consequently

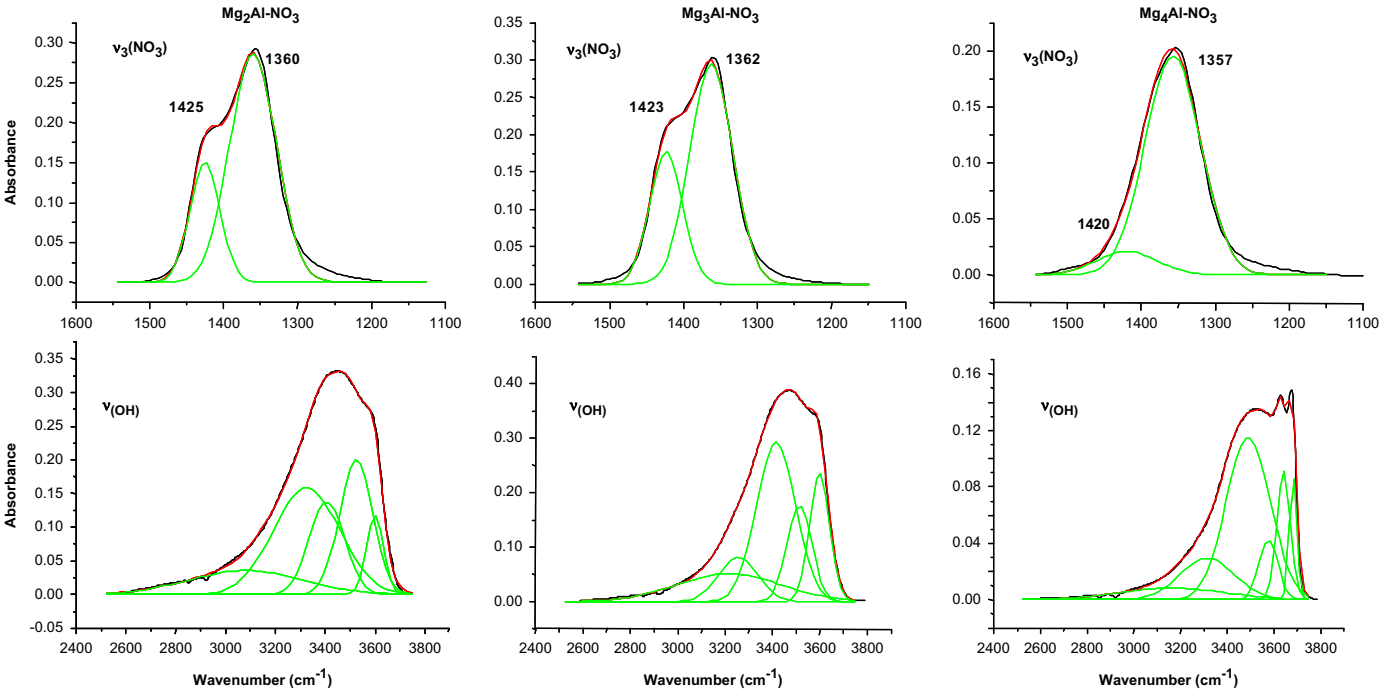

Fig. 2. ATR–FTIR spectra of Mg_2AlNO_3, Mg_3AlNO_3 and Mg_4AlNO_3 LDH adsorbents.

the ν_{MO} stretching bands are shifted toward lower energies (from 655 cm^{-1} for Mg_2Al and Mg_3Al to 590 cm^{-1} for Mg_4Al) as expected for a more ordered and rigid structure.

Textural properties of the LDH sorbents have been investigated by scanning electron microscopy, dynamic light scattering and N_2 adsorption isotherm BET analysis. LDH particles are formed by the aggregation of small platelets arranged in a sand-rose like morphology as shown on the SEM pictures (Fig.SI-2). We observed a clear increase of the platelet size with increasing Mg^{2+}/Al^{3+} molar ratio related to the improvement of cristallinity as mentioned above. However, the presence of both primary nanoparticles and aggregates leads to a bimodal particle size distribution, the fine fraction displaying a mean particle size of 602, 555 and 472 nm, respectively, for Mg_2AlNO_3, Mg_3AlNO_3 and Mg_4AlNO_3. All samples exhibit N_2 adsorption isotherms with hysteresis loops typical of inter-particle porosity between platelets (type H3) [29]. The BET specific surface area (Fig.SI-3) and porous volumes are low. A slight increase of S_{BET} is observed from Mg_2AlNO_3 (26 $m^2\,g^{-1}$) to Mg_3AlNO_3 (32 $m^2\,g^{-1}$) and Mg_4AlNO_3 (37 $m^2\,g^{-1}$) is in good agreement with particle size. Moreover, the increase in layer charge density from Mg_4Al to Mg_2Al favors the aggregation of platelets and the decrease of the specific surface area.

3.2. Thermodynamic study of OII adsorption by Mg_RAl LDH

Adsorption isotherms of OII molecules by Mg_RAlNO_3 at 25 °C are presented in Fig. 3. According to the classification proposed by Giles et al. [30], these isotherms correspond to the L-type (sub-group 2 or H) adsorption reactions and are observed when the adsorbent possesses a high affinity for the adsorbed molecules [31].

Plateau is reached in all cases at very low equilibrium concentration values (<0.5 mmol L^{-1}) and no further adsorption is found at higher concentrations (>4 mmol L^{-1}). This clearly indicates that the interactions between OII molecules and LDH are stronger than the sorbent–sorbent interactions. Quantification of dye removal by solids is of great importance for the development of clean processes. Moreover, from a fundamental point of view, the modelization of the adsorption phenomena may help to understand the molecule–solid interactions that occur at the liquid–solid interface and may also offer a deep insight into the characterization of these solid surfaces. Several models have been used to account for the adsorption behavior of solids. Some are thermodynamically consistent such as the Langmuir or the Henry models, which assume that the solid surface is homogeneous and displays a definite number of energetically equivalent and independent adsorption sites. Quantitative and energetic parameters

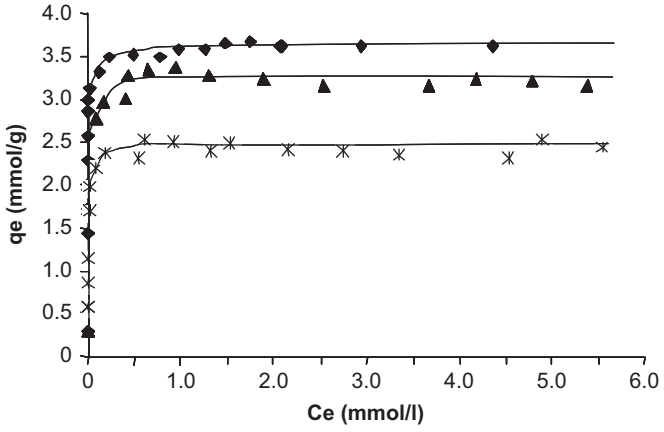

Fig. 3. OII adsorption isotherms for (♦), Mg_2AlNO_3, (▲) Mg_3AlNO_3, (x) Mg_4AlNO_3.

may then be extracted from the linear form of the Langmuir equation: $1/q_e = 1/q_{max} + (1/q_{max}K_L)(1/C_e)$, where q_e is the adsorbed dye concentration (mol g^{-1}), C_e the equilibrium dye concentration in the solution (mol L^{-1}), q_{max} the theoretical monolayer capacity and K_L is the constant related to the free energy of adsorption ($K_L \propto e^{-\Delta H/RT}$). At low equilibrium concentration, the non-linear form of the Langmuir equation may be approximated to the Henry's law:

$$q_e = \frac{q_{max}K_LC_e}{1+K_LC_e} \approx q_{max}K_LC_e$$

At high equilibrium concentration, a constant monolayer adsorption is predicted by the model. The essential feature of the Langmuir isotherm can be expressed in terms of a dimensionless constant separation factor for equilibrium parameter, R_L [32] which is defined by $R_L = 1/1 + K_LC_0$, where C_0 is the highest initial concentration, K_L the Langmuir constant and R_L indicates the shape of the isotherm as follows (Table SI-1).

Generally, there is a relation between the degree of reliability and the irreversibility of the phenomenon, giving a qualitative assessment of adsorbate–sorbent interactions. The R_L factor tends from unity to zero when changing from a completely reversible phenomenon to a completely ideal irreversible adsorption.

The Freundlich model has been largely developed to account for deviation to the Langmuir behavior. It gives a more realistic description of non-ideal solid surfaces even though it suffers from a lack of thermodynamic relevance. The Freundlich model considers that the presence of heterogeneities causes a non-uniform distribution of adsorption heat over the surface. More specifically, this models supposes a logarithmic decrease of the adsorption heat, under surface coverage. The slope ($1/n_f$) of the linear form of the Freundlich equation ($\log Q = \log K_f + (1/n_f)\log C_e$) indicates the level of surface heterogeneity. K_f gives estimates of the adsorption capacity while n_f is a measure of the interaction intensities. It is comprised between 0 and 1. Cooperative adsorption will be definite by a value of $1/n_f$ larger than 1.0. The Freundlich model is largely used to fit adsorption data of dye molecules or pesticides on various sorbents [15].

Several other models have been developed to optimize the description of molecular adsorption onto solids. The Tempkin model considers that adsorbate–adsorbate interactions cause a linear decrease of the adsorption energy: $q_e = (RT/b)\ln AC_e$, where RT/b is related to the heat of adsorption.

In this study, the adsorption isotherms of OII by Mg_RAlNO_3 LDH were processed according to the various models presented above. Our data satisfactorily fit the Langmuir model with R^2 values almost always equal to 0.999 (Table 3). Modeling the adsorption isotherms with the herein mentioned models gave unrealistic worst fit results. Adsorption of dye molecules by charcoals [33], biomass [34], chitosan [35], activated sludge [36] fly-ashes [37] or clays [38] have also been deeply investigated using several adsorption models. All these solids display interesting adsorption properties but they are known to exhibit a lot of chemical and physical heterogeneities rendering the modeling study difficult. Layered Double Hydroxides are very interesting models of solids because they are synthetic materials which can be prepared with a tight control of their chemical and textural properties. Their high chemical and physical homogeneity may explain then their ideal behaviors for adsorption.

Mg_2AlNO_3 displays the highest adsorption capacity with 3.611 mmol of OII per gram of Mg_2AlNO_3 at 40 °C. Here, we observed better sorption abilities for OII than any other materials reported in the literature [19,20,33,35–37,39,40] (Table SI-2). Marangoni et al. [41] have recently reported values of adsorption of Evans Blue, Chicago Sky Blue 6B and Niagara Blue 3B by Zn_2Al–Cl LDH much lower than what we obtained in this study. This may

Table 3
Langmuir parameters for adsorption isotherms of OII by Mg_RAlNO_3 at 10, 25 and 40 °C.

Langmuir constants									
LDH	$Q_m \times 10^{-3}$ (mol/g) (% A.E.C.)			$K_L \times 10^{-3}$ (L/mol)			R^2		
	10 °C	25 °C	40 °C	10 °C	25 °C	40 °C	10 °C	25 °C	40 °C
Mg_2AlNO_3	3.374 (90.3%)	3.529 (94.4%)	3.611 (96.6%)	109.740	466.833	1384.5	0.999	0.999	0.999
Mg_3AlNO_3	2.976 (98.6%)	3.272 (108.4)	3.434 (113.8%)	71.493	203.73	269	0.999	0.999	0.998
Mg_4AlNO_3	1.929 (78.5%)	2.637 (107.3)	2.914 (118.5%)	8.073	70.222	142.958	0.997	0.999	0.999

be explained by the voluminous molecular structures of these dyes, which cannot be adsorbed to the full anion exchange capacity of the materials.

Moreover, adsorption capacities (Q_m) and LDH–OII affinities (K_L) are strongly dependent on the Mg^{2+}/Al^{3+} ratio (i.e. on the charge density of the layers). The adsorbed concentration at the plateau level increases in the order $Mg_4AlNO_3 < Mg_3AlNO_3 < Mg_2AlNO_3$, respectively, as the charge per unit surface $2.47 < 3.12 < 4.26$ e/nm^2 of the solids increases, whatever the equilibrium temperature. Chemical analyses of solutions after adsorption equilibrium shows that nitrate release is proportional to the OII uptake, indicating that adsorption occurs through an anionic exchange mechanism. In most of the cases, maximum adsorption capacities of the various solids reach more than 90% of the anion exchange capacities (Table 3). Regardless of the Mg/Al ratio, the adsorption capacity of OII is under its full anion exchange capacity at 10 °C, but at 25 and 40 °C, Mg_3AlNO_3 and Mg_4AlNO_3 adsorb O-II more than their full anion exchange capacity. Slight variation of the textural properties between the sorbents does not affect the thermodynamic of this exchange process but only influences the kinetic of diffusion of the anionic species. However kinetic still remains very fast for all three sorbents (data not shown).

Effect of pH on the adsorption capacity of Mg_2AlNO_3 has been measured (Fig. 4) in order to determine the stability of the sorbent and in order to investigate its effect on the chemical process. The adsorption capacity was found to be constant over a large range of pH from acidic condition (pH=4.0) to more basic medium (pH=10.0), as expected for an anion exchange reaction, which is independent of the proton concentration. Moreover, this behavior confirms the high stability of the LDH phases in terms of solubility, showing the advantage of using these materials in water treatments under a large range of pH conditions. At higher pH value (> 10.0), the decrease in adsorption is mainly due to competition with carbonate intercalation.

Influence of temperature on the dye adsorption was also investigated (Fig. 5). Not only does the increase in temperature fasten the diffusion of the dye molecule in the internal and external pores of the sorbents but it also affects the adsorption equilibrium and consequently the total adsorption capacity. Results show that the capacity of adsorption increases with increasing temperature for all Mg/Al composition with a maximum at 40 °C.

Figure SI-4 presents the calculated R_L value versus temperature for the different phases. It is observed that R_L values are in the range 0–1 in all cases. These results are relevant to a Langmuir behavior with a great LDH-Dye affinity. Increase of the layer charge from Mg_4Al to Mg_2Al results in more energetic sites, as evidenced by the decrease in R_L value.

The evolution of the R_L value with M^{II}/M^{III} ratio is then explained by the enhancement of the global affinity of the layers toward the dye anions, increasing the irreversibility of the phenomenon. On the other hand, R_L decreases nearly linearly with temperature of adsorption. The slope being similar, all LDH sorbents undergo the same thermal activation. This behavior accounts for an endothermic adsorption phenomenon. It can be noted that at 40 °C, very low R_L values are reached. With $R_L=0.112$, Mg_2AlNO_3 adsorbs OII almost irreversibly. Thermodynamic parameters may be estimated by using the Langmuir

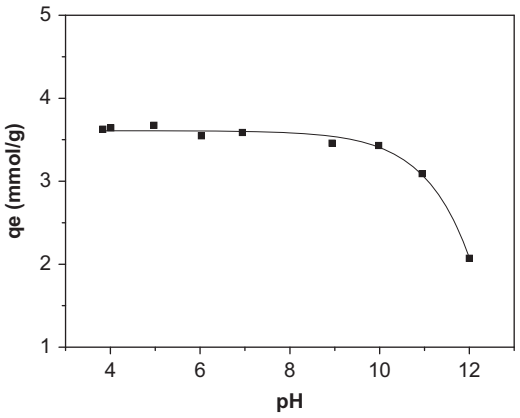

Fig. 4. pH dependence of OII adsorption by Mg_2AlNO_3 (C_i=2 g/l, T=25 °C).

constants K_L and its dependence with temperature according to the following relations :

$$\Delta G^\circ = -\,\mathrm{RTLn}K_L \text{ and } \mathrm{Ln}K_L = -\Delta G^\circ/\mathrm{RT} = -\Delta H^\circ/\mathrm{RT} + \Delta S^\circ/R$$

where ΔH° is the change in enthalpy of the adsorption reaction, ΔS° is the change in entropy and ΔG° is the change in Gibb's free energy [42]. The values of ΔG°, ΔH° and ΔS° obtained from our experiments were calculated plotting $\mathrm{Ln}K_L$ versus $1/T$ and are reported in Table 4.

The negative values of ΔG° suggest the spontaneous nature of OII adsorption by LDH. Changes in ΔG° with M^{II}/M^{III} ratio and temperature confirm the trends in affinity of Mg_RAlNO_3 for OII as already mentioned. The change of enthalpy was found to be positive, confirming the endothermic nature of adsorption. In general, a high enthalpy change may show chemisorption (40–120 kJmol^{-1}) rather than physisorption (< 40 kJmol^{-1}), but the reverse is not true. A small enthalpy, even endothermic, may also correspond to a chemisorption, thus the adsorption of OII on LDH would be likely due to chemisorption according to this model. However, the calculated ΔH° values do not follow a coherent trend in the Mg_RAlNO_3 series, even though a high experimental reproducibility was obtained for the isotherm data points (deviation less than 3%). At that point of data processing, it appears that determination of enthalpy values using the Langmuir model is maybe not so adequate, showing some limitations of such theoretical approach.

Positive values of ΔS° indicate the increasing randomness at the solid/liquid interface and the high affinity of the adsorbent toward OII [23,43,44].

3.3. OII–LDH interactions: structural insight in the adsorption mechanism

All three Mg_RAlNO_3 (R=2, 3, 4) sorbents undergo a structural modification at very low concentration of OII, as shown on the X-ray diffractograms (Fig.6). A second series of seven (0 0 l) diffraction lines, characteristic of LDH–OII phases with expended

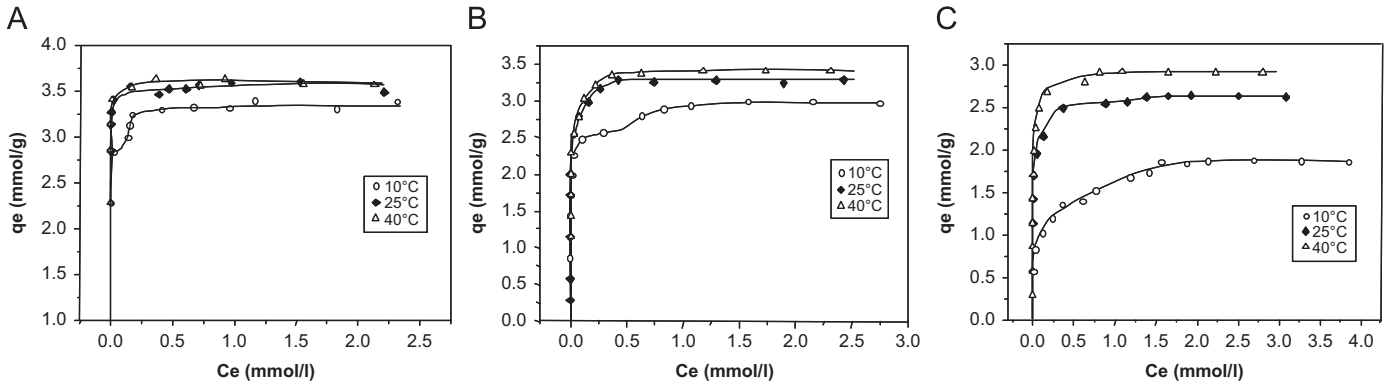

Fig. 5. OII adsorption isotherms for (A) Mg_2AlNO_3, (B) Mg_3AlNO_3 and (C) Mg_4AlNO_3 at 10, 25 and 40 °C.

Table 4
Calculated thermodynamic parameters from the Langmuir model.

Thermodynamic constants					
LDH	$-\Delta G^\circ$ (kJ mol^{-1})			ΔH° (kJ mol^{-1})	ΔS° (J K^{-1})
	10 °C	25 °C	40 °C		
Mg_2AlNO_3	−11.05	−15.22	−18.82	62.32	259.59
Mg_3AlNO_3	−10.04	−13.17	−14.56	32.82	152.38
Mg_4AlNO_3	−4.91	−10.53	−12.91	71.09	270.29

basal spacings of about 2.220 nm, appears beside the (0 0 3) and (0 0 6) peaks of the nitrate phases. The diffraction lines of the nitrate containing LDH disappear simultaneously with the increase of the intensities of the new Bragg reflections. For both Mg_2AlNO_3 and Mg_3AlNO_3, nitrate anions are fully exchanged for OII initial concentration of 1.42 mM, while for Mg_4AlNO_3 some precursor material is still present at the OII saturation. The same $d_{1\,1\,0}$ distance is retained for all phases after adsorption, showing that adsorption proceeds through a topotactic anion exchange reaction, without any change of the layer structure. Values of the gallery heights calculated from the experimental basal spacings are centered around 1.740 nm, typical of OII containing Mg_RAl LDH phases with OII anions (larger dimension: 1.356 nm) orientated nearly perpendicularly to the layer. The infrared study (Fig.7) is in good agreement with the PXRD data. Typical vibration bands of the OII molecule appear early in the adsorption process. The intensity of the $\nu_3(NO_3)$ antisymmetric stretching band of the nitrate anion decreases progressively until disappearance for Mg_2AlNO_3 and Mg_3AlNO_3, while residue of nitrate band is still present for Mg_4Al at saturation. Positions of the lattice vibrations and vibration bands of OII anion are not affected by intercalation.

UV–vis spectra of Mg_RAlNO_3 ($R=2$, 3, 4) with increasing amount of adsorbed OII are presented in Fig. 8. Two absorption bands appear in the 350–550 nm region. The two bands relative intensities depend on the amount of adsorbed dye molecule. Orange II is known to adopt two tautomeric forms in solution, the azonaphtol (AZO) and quinone hydrazone (HYD) forms (Fig. SI-1), as reported in the literature [45]. Absorption maxima in the visible region of the AZO and HYD forms are, respectively, pointed at 401 and 483 nm. Obviously, an equilibrium between both forms exist, in the solids.

At low adsorption concentrations (<200 mg/g), OII adsorbs onto the LDH in the AZO form, while at higher concentrations this is the HYD tautomer, which is better stabilized. The AZO–HYD transition appears at higher loading for Mg_2Al than Mg_4Al. At adsorption concentration equal to Q_m, only the HYD form is evidenced, as for the pure OII intercalated Mg_RAl coprecipitated LDH phases (data not shown). However both LDH phases intercalated either by the azo or the hydrazo forms display similar X-ray diffractograms, indicating a similar arrangement of both anion in the interlayer galleries. Surprisingly, FTIR spectra are not affected by this tautomeric transition. This tautomeric evolution could be explained by a slight conformational change of OII anion under intercalation, facilitating the proton transfer from the hydroxo to the azo group. Adsorptions of OII by Mg_RAlNO_3 LDH were monitored by zetametry (Fig. 9) in order to sort out the localization of OII molecules under the adsorption process. Due to the positive charge of their layers, Mg_RAlNO_3 LDH materials display positive zeta potential (ζ), 34.2, 42.5 and 30.6 mV, respectively, for $R=2$, 3 and 4. Adsorption at low concentration of OII by Mg_2AlNO_3 and Mg_3AlNO_3 leaves this value almost unaffected. As shown by the XRD data, at such early steps of adsorption, OII molecules intercalate in the structure or diffuse inside the aggregates without changing the composition of the external Stern double layer of the secondary particles.

At 49% and 70% of the total adsorption capacity (respectively, for Mg_2AlNO_3 and Mg_3AlNO_3), adsorption of OII starts to modify the external surface and the ζ value decreases up to the total inversion of charge (-27.2 mV ($R=2$) and -28.1 mV ($R=1$)). Behavior of Mg_4AlNO_3 is clearly different. In this case, the zeta potential decreases nearly continuously from very low initial OII concentrations. This decrease may be explained by the lower reactivity of Mg_4Al toward intercalation by anion exchange as confirmed by XRD and ATR–FTIR results. Until $C_i=0.285$ mmol/L, only the external surface of aggregates is modified by adsorption, no intercalation occurs. At higher concentration values, the slow-down of ζ change indicates that OII intercalation by anionic exchange becomes effective. The results of zetametry analysis are in good agreement with calorimetric data. In the case of Mg/Al=2 or 3, the adsorption enthalpy is initially constant and corresponds to the intercalation of OII, whereas, in the case of Mg/Al=4, the adsorption probably occurs both on the external surface and by anion exchange reaction (intercalation) from the beginning, leading to a decrease of adsorption enthalpy with coverage.

4. Conclusion

The above results permit to conclude that Mg_RAlNO_3 LDH exhibit very high adsorption properties for the removal of O-II from water.

The O-II adsorption isotherms of Mg_RAl–NO_3–LDH ($R=2$, 3, 4) showed that the adsorption capacity increases with the layer charge density. Adsorption isotherms could be fitted according to

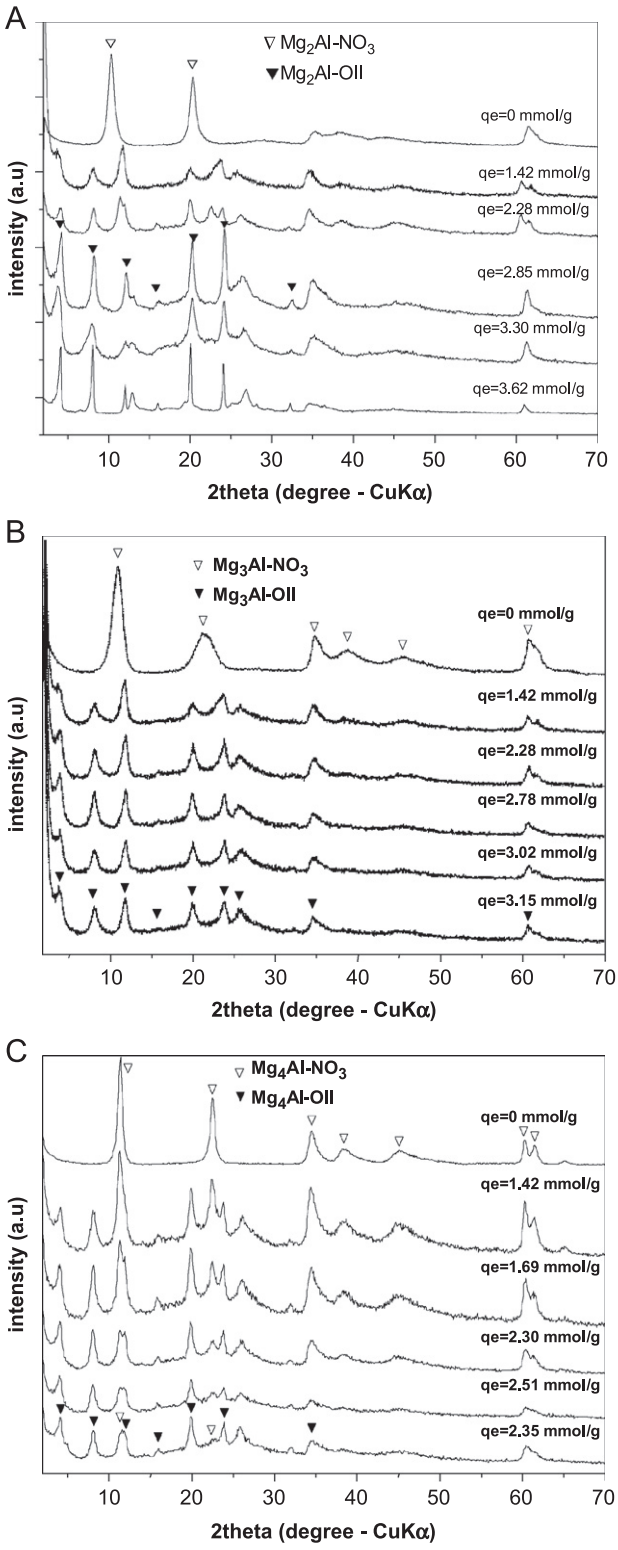

Fig. 6. XRD patterns for (A) Mg_2AlNO_3, (B) Mg_3AlNO_3 and (C) Mg_4AlNO_3 LDH before and after adsorption at different initial concentrations of OII (C_i). The corresponding adsorbed amounts of OII (q_e) are also given.

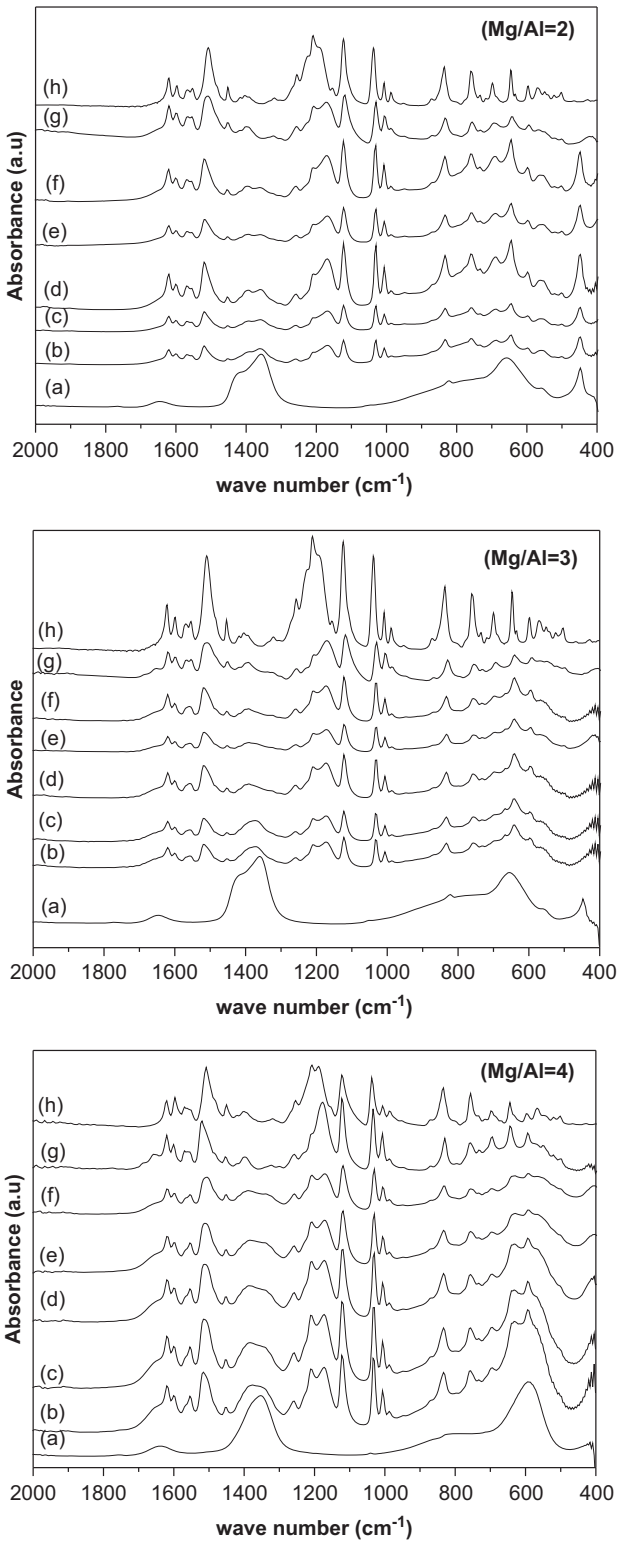

Fig. 7. ATR–FTIR spectra for (a) $Mg_RAl–NO_3$ (R=2,3,4) and $Mg_RAl–NO_3$ (R=2,3,4) after OII adsorption (b) C_i=1.42 mmol/l; (c) C_i=2.28 mmol/l; (d) C_i=2.85 mmol/l; (e) C_i=3.42 mmol/l; (f) C_i=5.7 mmol/l and (g) Mg_2–Al–OII; (h) OII.

the Langmuir equation. High R_L values indicate a high affinity of LDH sorbents for OII. The negative values of Gibbs free energies (ΔG°) demonstrate that the O-II adsorption is spontaneous and favoured when increasing temperatures. The combination of PXRD, FTIR, UV–vis and Zetametry characterization techniques evidence that the adsorption of OII proceeds via an anion exchange reaction either at the surface or in the interlayer domains. The chemical stability of Mg_RAlNO_3 LDH over a large range of pH suggests that these materials could be good adsorbents for aqueous dyes in contaminated water.

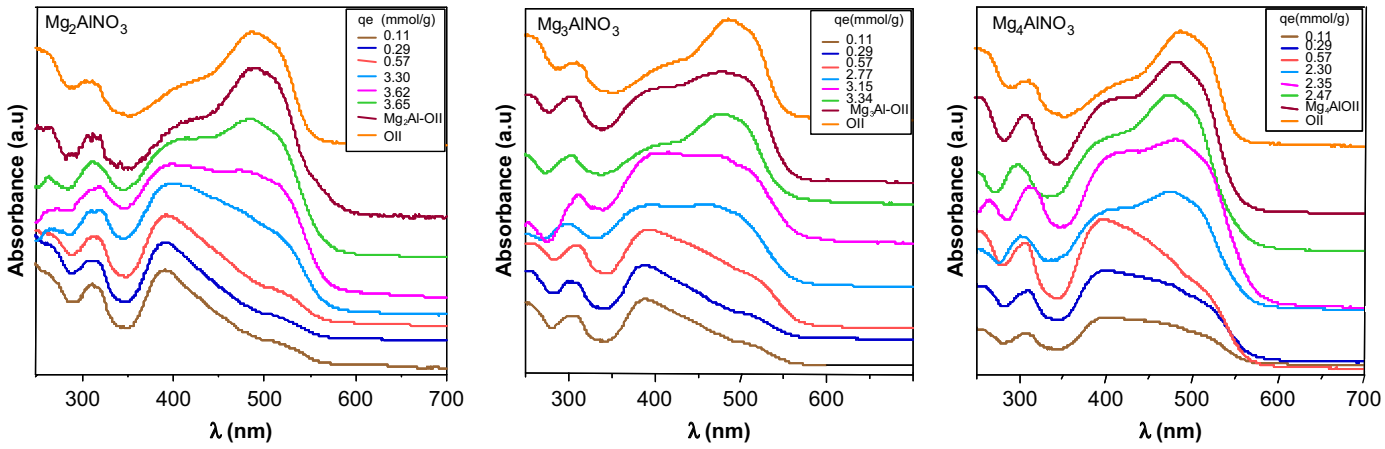

Fig. 8. Reflectance UV–Visible spectra for LDH and LDH naocomposites Mg_RAl (R=2, 3, 4) before and after adsorption at different initial concentrations of OII (C_i). The corresponding adsorbed amounts of OII (q_e) are also given.

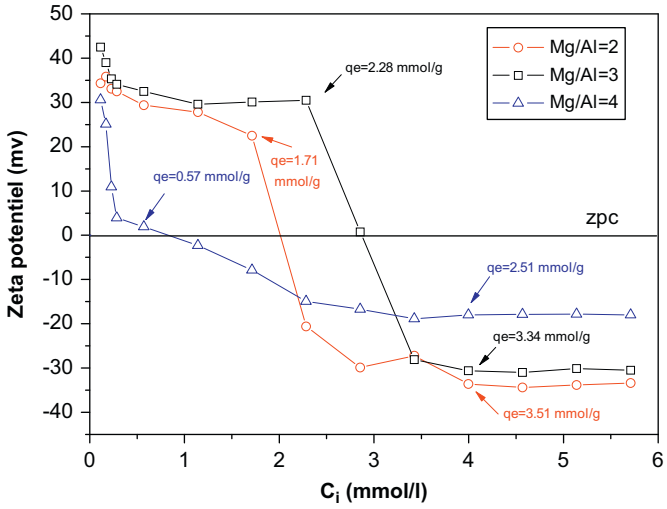

Fig. 9. Zeta potential of Mg_RAlNO_3 at various OII initial concentration C_i.

Aknowledgments

The authors thank the PHC program Tassili 06MDU676, ruled out under the French-Algerian scientific cooperation for supporting these researches.

Appendix A. Supplementary material

Supplementary data associated with this article can be found in the online version at doi:10.1016/j.jssc.2011.03.018.

References

[1] A.K. Mittal, C. Venkobachar, Studies on sorption of dyes by sulfonated coal and Ganoderma lucidum, Indian J. Environ. Health 31 (1989) 105–111.
[2] R. Sivaraj, C. Namasivayam, K.T. Kadirvelu, Orange peel as an adsorbent in the removal of Acid violet 17 (acid dye) from aqueous solutions, Waste Manag 21 (2001) 105–110.
[3] Y. Al-Degs, M.A.M. Khraisheh, S.J. Allen, M.N.A. Ahmad, Sorption behavior of cationic and anionic dyes from aqueous solution on different types of activated carbons, Sep. Sci. Technol. 36 (2001) 91–102.
[4] P. Janoš, H. Buchtová, M. Rýznarová, Sorption of dyes from aqueous solutions onto fly ash, Water Res. 37 (2003) 4938–4944.
[5] G. Mckay, V.J.P. Poots, Kinetics and diffusion processes in colour removal from effluent using wood as an adsorbent, J, Chem. Technol. Biotechnol. 30 (1980) 279–292.
[6] C. Namasivayam, N. Kanchana, Removal of congo red from aqueous solution by waste banana pith, Pertanika, J. Sci. and Technol. 1 (1993) 33–42.
[7] A.S. Özcan, A. Özcan, Adsorption of acid dyes from aqueous solutions onto acid-activated bentonite, J. Colloid Interf. Sci. 276 (2004) 39–46.
[8] C.C. Wang, L.C. Juang, T.C. Hsu, C.K. Lee, J.F. Lee, F.C. Huang, Adsorption of basic dyes onto montmorillonite, J. Colloid Interf. Sci. 273 (2004) 80–86.
[9] S. Kacha, M. Ouali, S. Elmaleh, Élimination des colorants des eaux résiduaires de l'industrie textile par la bentonite et des sels d'aluminium, Rev. Sci. Eau. 10 (1997) 233–248.
[10] R.S. Juang, F.C. Wu, R.L. Tseng, The ability of activated clay for the adsorption of dyes from aqueous solutions, Environ. Technol. 18 (1997) 525–531.
[11] N.M. Mamdouh, M.S. El-Geundi, Comparative cost of colour removal from textile effluents using natural adsorbents, J. Chem. Technol. Biotechnol. 50 (1991) 257–264.
[12] S. Miyata, Physico-chemical properties of synthetic hydrotalcites in relation to composition, Clays Clay Miner. 28 (1980) 50–55.
[13] S. Miyata, Anion-exchange properties of hydrotalcite-like compounds, Clays Clay Miner. 31 (1983) 305–311.
[14] V. Rives, Layered Double Hydroxides: Present and Future, Nova Sci. Pub., Inc., New York, 2001.
[15] C. Forano, Environmental remediation involving layered double hydroxides in Clay Surfaces, in: F. Wypych, K.G. Satyanarayana (Eds.), Fundamentals and Applications, Elsevier Academic Press, New York, 2004, pp. 425–458.
[16] M. Morigi, E. Scavetta, M. Berrettoni, M. Giorgetti, D. Tonelli, Sulfate-selective electrodes based on hydrotalcites, Anal. Chim. Acta 439 (2001) 265–272.
[17] S. Vial, C. Forano, D. Shan, C. Mousty, H. Barhoumi, C. Martelet, N. Jaffrezic, Nanohybrid-layered double hydroxides/urease materials: synthesis and application to urea biosensors, Mater. Sci. Eng. C 26 (2006) 387–393.
[18] M. Webb, Special Publication-RSC, Ion Exchange Developments and Applications, Cambridge 182 (1996) 135.
[19] U. Costantino, N. Coletti, M. Nocchetti, G.G. Aloisi, F. Elisei, L. Latterini, Surface Uptake and Intercalation of Fluorescein Anions into Zn – Al – Hydrotalcite: Photophysical Characterization of Materials Obtained, Langmuir 16 (2000) 10351–10358.
[20] N.K. Lazaradis, T.D. Krapantsis, D. Georgantas, Kinetic analysis for the removal of a reactive dye from aqueous solution onto hydrotalcite by adsorption, Water Res. 37 (2003) 3023–3033.
[21] M.X. Zhu, Y.P. Li, M. Xie, H.Z. Xin, Sorption of an anionic dye by uncalcined and calcined layered double hydroxides: a case study, J. Hazard. Mater. 120 (2005) 163–171.
[22] J. Orthman, H.Y. Zhu, G.Q. Lu, Use of anion clay hydrotalcite to remove coloured organics from aqueous solutions, Sep. Purif. Technol. 31 (2003) 53–59.
[23] A. de Roy, Lamellar double hydroxides, Mol. Cryst. Liq. Cryst. 311 (1998) 173–193.
[24] A. Vaccari, Clays and catalysis: a promising future, Appl. Clay Sci. 14 (1999) 161–198.
[25] F. Cavani, F. Trifiro, A. Vaccari, Hydrotalcite-type anionic clays: preparation, properties and applications, Catal. Today 11 (1991) 173–301.
[26] A. de Roy, C. Forano, M. El Malki, J.P. Besse, Anionic clays: trends in pillaring chemistry, in: M.L. Occelli, H.E. Robson (Eds.), Synthesis of Microporous Materials, Expanded Clays and Other Microporous Solids, Van Nostrand Reinhold, New York, 1992, pp. 108–170.
[27] R. Denoyel, F. Giordano, J. Rouquerol, Thermodynamic study of non-ionic—anionic surfactant mixtures: micellization and adsorption on silica, Colloids Surf. 76 (1993) 141–148.

[28] A. Drits, A.S. Book, V. Rives (Eds.), Layered Double Hydroxides: Present and Future, Nova Sci. Pub. InC, New York, , 2001 Chap. 2.
[29] F. Rouquerol, J. Rouquerol, K.S.W. Sing, Adsorption by Powders and Porous Solids, Academic Press, London, 1999.
[30] C.H. Giles, D. Smith, A. Huitson, A general treatment and classification of the solute adsorption isotherm. I. Theoretical, J. Colloid Interf. Sci. 47 (1974) 755–765.
[31] R. Calvet, Adsorption of organic chemicals in soils, Environ. Health Perspective 83 (1989) 145–177.
[32] R. Hall, L.C. Eagleaton, A. Acrivos, T. Vermeulen, Pore- and Solid-Diffusion Kinetics in Fixed-Bed Adsorption under Constant-Pattern Conditions, Ind. Eng. Chem. Fundam. 5 (1966) 212–223.
[33] J.I. Muhammad, N.A. Muhammad, Adsorption of dyes from aqueous solutions on activated charcoal, J. Hazardous Mater. 139 (2007) 57–66.
[34] T.V.N. Padmesh, K. Vijayaraghavan, G. Sekaran., M. Velan, Application of *Azolla rongpong* on biosorption of acid red 88, acid green 3, acid orange 7 and acid blue 15 from synthetic solutions, Chem. Eng. J. 122 (2006) 55–63.
[35] P. Janos, H. Buchtova, M. Ryznarova, Sorption of dyes from aqueous solutions onto fly ash, J. Water Res. 37 (2003) 4938–4944.
[36] S.S. Tahir, N. Rauf, Removal of a cationic dye from aqueous solutions by adsorption onto bentonite clay, Chemosphere 63 (2006) 1842–1848.
[37] Y.C. Wong, Y.S. Szeto, W.H. Cheung, G.J. Mc Kay, Equilibrium studies for acid dye adsorption onto chitosan, Langmuir 19 (2003) 7888–7894.
[38] S.A. Ong, E. Toorisaka, H.M.H. Tadashi, Treatment of azo dye Orange II in aerobic and anaerobic-SBR systems, Process Biochem. 40 (2005) 2907–2914.
[39] V.K. Gupta, A. Mittal, V. Gajbe, J. Mittal, Removal and recovery of the hazardous azo dye acid orange 7 through adsorption over waste materials: bottom ash and de-oiled soya, Ing. Eng. Chem. Res. 45 (2006) 1446–1453.
[40] U. Costantino, N.J. Coletti, Anion exchange of methyl orange into Zn – Al Synthetic hydrotalcite and photophysical characterization of the intercalates obtained, Langmuir 15 (1999) 4454–4460.
[41] R. Marangoni, M. Bouhent, C. Taviot-Guého, F. Wypych, F. Leroux, Zn_2Al layered double hydroxides intercalated and adsorbed with anionic blue dyes: a physico-chemical characterization, J. Coll. Interf. Sci. 333 (2009) 120–127.
[42] S. Tunali, A. Safa Ozcan, A. Ozcan, T. Gedikbey, Kinetics and equilibrium studies for the adsorption of Acid Red 57 from aqueous solutions onto calcined-alunite, J. Hazardous Mater. 135 (2006) 141–148.
[43] Q. Hu, Z. Xu, S. Qiao, F. Haghseresht, M. Wilson, G.Q. Lu, J Colloid Interf. Sci. 308 (2007) 191.
[44] F. Renault, N. Morin-Crini, F. Gimbert, P. Badot, G. Crini, Bioresour. Technol. 9 (2008) 7573.
[45] J.N. Ospenson, J. Some, Studies on Azo Dyes. II, Acta Chem. Scand. 5 (1951) 491–497.